Chapter 15

Numerical Simulation of Nanoparticles with Variable Viscosity over a Stretching Sheet

Noreen Sher Akbar, Dharmendra Tripathi and Zafar Hayat Khan

Additional information is available at the end of the chapter

http://dx.doi.org/10.5772/intechopen.71224

Abstract

The effects of different types of base fluids on carbon nanotube (CNT) nanofluids flow over a circular stretching sheet are numerically analyzed. The nonlinear variation of radial velocity in radial direction is assumed at surface of stretching sheet. The temperature dependent fluid viscosity is taken into consideration. Two different types of flows (assisting flow and opposing flow) are discussed under the buoyant force effects. Single walled CNT and multi walled CNT are considered as nanoparticles for better thermal conductivity of the nanofluids. A set of similarity transformations to convert the partial differential equations into ordinary differential equations is hired. The non-linear ODEs are numerically solved by employing fourth order Runge-Kutta method. Discussions of numerical simulations for flow characteristics have been made appropriately. A comparative study for various type of base fluids like kerosene, engine oil and ethylene glycol is also presented. From the predicted simulation, it is observed that the variation in Nusselt number is maximum for engine oil and minimum for kerosene oil however, the variation in skin friction coefficient is largest for kerosene oil and least for engine oil. Furthermore, numerical results are also validated with achieving a good correlation with existing results.

Keywords: CNT nanofluids, nonlinear stretching sheet, Runge-Kutta method, buoyancy force, heat transfer, similarity transformation

1. Introduction

The first key point of present investigation is carbon nanotubes (CNTs) nanofluids that means the suspension of CNTs in conventional fluids such as air, helium, water, minerals oils, Freon, and ethylene glycol. The applications of nanofluids spread over a wide range of disciplines, including heat transfer, material science, physics, and chemical engineering. Many techniques have been used to enhance the thermal conductivity of the base fluids in which the suspension

of micro/nano-sized particles in fluids have also been tried since many decades. However, the word 'nanofluids' was primarily introduced by Choi [1]. He has studied the thermal conductive effects on convectional fluids subject to suspension of metallic nanoparticles. He has observed that with suspension of nanoparticles, the thermal conductivity of convectional fluids enhances. In these directions, numerous investigations have therefore been carried out in the past few decades, seeking to wide applications and developments, some interesting reviews [2–4] have been reported.

To study the heat transfer rate of water based nanofluids, the various types of nanoparticles like titanium dioxide, alumina, silica diamond, zinc-oxide and copper [5–7] have been considered. It has been depicted that the thermal conductivity enhances with suspension of the nanoparticles. Moreover, CNTs have also received great interest due to significant enhancement of thermal conductivity, unique structure and physical (mechanical and electrical) properties [8, 9]. Ding et al. [8] have prepared a nanofluids with suspension of CNTs in distilled water and measured the thermal conductivity and viscosity of CNTs nanofluids. They have reported the enhancement of thermal conductivity depends on CNTs concentration, and pH level. They also concluded that nanofluids with 0.5 wt.% CNTs, the maximum enhancement is over 350% at Re = 800. Ko et al. [9] experimentally reported the flow characteristics of CNTs nanofluids in a tube and summarized that the friction factor for CNT nanofluid is low in compare to water. Another experimental study for thermophysical properties of CNTs nanofluids with base fluid as mixture of water and ethylene glycol has been presented by Kumaresan and Velraj [10]. And this study noted that the maximum thermal conductivity enhances up to 19.75% for the nanofluid containing 0.45 vol.% MWCNT at 40°C. In addition, few more experimental investigations [11, 12] with applications in a tubular heat exchanger of various lengths for energy efficient cooling/heating system and turbulent flow heat exchanger are performed. With CNTs nanofluids, some more numerical simulations [13, 14] for flow characteristics are presented in literature and discussed the physiological flows application.

The second key point is boundary layer flow over a circular stretching sheet. The boundary layer flow past a stretching sheet was initially investigated by Crane [15]. He has discussed its applications such as annealing and tinning of copper wires, polymer extrusion in melt spinning process, manufacturing of metallic sheets, paper production, and glass, fiber and plastic production etc. The heat transfer rate play important role in all manufacturing, productions and fabrication processes. This model has been explored by many investigators for various physical aspects. However, some interesting extensions of Crane's model for boundary layer flow of nanofluids have recently investigated, see examples [16–30]. The first boundary layer flow model for nanofluids flow past stretching sheet was presented by Khan and Pop [16] which was extended for a convective boundary condition [17], nonlinear stretching sheet [18], unsteady stretching surface [19], micropolar nanofluid flow [20], magneto-convective non-Newtonian nanofluid slip flow over permeable stretching sheet [21], Non-aligned MHD stagnation point flow of variable viscosity nanofluids [22], Stagnation electrical MHD mixed convection [23], exponential temperature-dependent viscosity and buoyancy effects [24], thermo-diffusion and thermal radiation effects on Williamson nanofluid flow [25], magnetic dipole and radiation effects on viscous ferrofluid flow [26], transient ferromagnetic liquid flow [27], magnetohydrodynamic Oldroyd-B nanofluid [28],

http://dx.doi.org/10.5772/intechopen.71224

spherical and non-spherical nanoparticles effects [29], three dimensional free convective magnetohydrodynamics [30]. Moreover, some works [31–34] extended Khan and Pop's model for CNTs nanofluids where combined effects of slip and convective boundary conditions have been discussed [31], convective heat transfer in MHD slip flow has been studied [32], nonlinear stretching sheet with variable thickness has been considered [33] and variable thermal conductivity and thermal radiation effects have been discussed.

After reviewed many investigations [16–34] on boundary layer flow of nanofluids past through linear/nonlinear stretching sheet, none of the them has been reported for boundary layer flow of CNTs nanofluids over a circular stretching sheet. Considering this gap of research, we formulate a model and also numerically simulate it to study the flow characteristic of CNTs nanofluids flow over a circular stretching sheet. Kerosene, Engine oil and Ethylene glycol are considered for base fluids. And MCNT and SWCNT are also taken as nanoparticles. The negative and positive buoyant force effects as opposing and assisting flows are also examined. The effects of fluid and flow parameters on velocity profile, temperature profile, skin-friction coefficient, Nusselt number and stream lines are computed numerically.

2. Mathematical model

We consider the laminar incompressible flow of CNTs nanofluids over a circular sheet aligned with the $r\theta$-plane in the cylindrical coordinate system (r, θ, z). The schematic representation and coordinate system are depicted in **Figure 1**.

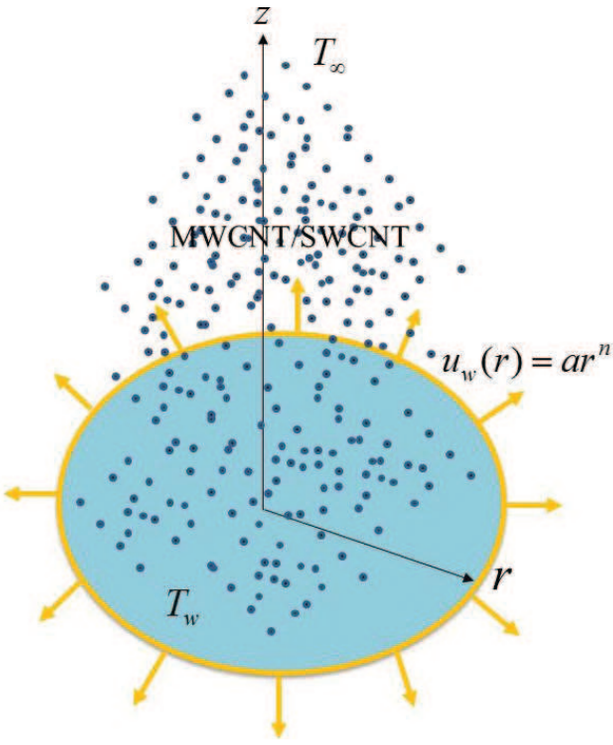

Figure 1. Schematic representation of CNTs nanofluids flow over circular stretching sheet.

The flow regime is considered as in the half space $z \geq 0$ and the sheet is stretched in radial direction with polynomial variation. The temperature at sheet is fixed as T_w and ambient temperature is considered as T_∞. Considering the boundary layer flow assumptions, the governing equations for conservation of mass, momentum, and energy can be expressed as:

$$\frac{\partial u}{\partial r} + \frac{u}{r} + \frac{\partial w}{\partial z} = 0, \tag{1}$$

$$\left(u\frac{\partial u}{\partial r} + w\frac{\partial u}{\partial z}\right) = \frac{1}{\rho_{nf}}\frac{\partial}{\partial z}\left(\mu_{nf}(T)\frac{\partial u}{\partial z}\right) \pm g\beta(T - T_\infty), \tag{2}$$

$$\left(u\frac{\partial T}{\partial r} + w\frac{\partial T}{\partial z}\right) = \alpha_{nf}\frac{\partial^2 T}{\partial z^2}, \tag{3}$$

where u and w are the velocity components along r- and z-directions respectively, T is the temperature. Here the "+" sign in Eq. (2) corresponds to the assisting flow while the "−" sign corresponds to the opposing flow, respectively. Here, ρ_{nf} is the nanofluid density, k_f is the thermal conductivity of the fluid, T_w is the wall temperature, $\mu_{nf}(T)$ is the temperature dependent viscosity of nanofluid and α_{nf} is the thermal diffusivity of nanofluid which are defined [31–34] as:

$$\mu_{nf} = \frac{\mu_0 e^{-\alpha\theta}}{(1-\phi)^{2.5}}, \tag{4a}$$

$$\alpha_{nf} = \frac{k_{nf}}{(\rho c_p)_{nf}}, \qquad \rho_{nf} = (1-\phi)\rho_f + \phi\rho_s, \tag{4b}$$

$$(\rho c_p)_{nf} = (1-\phi)(\rho c_p)_f + \phi(\rho c_p)_s, \tag{4c}$$

$$(\rho\gamma)_{nf} = (1-\phi)(\rho\gamma)_f + \phi(\rho\gamma)_S, \tag{4d}$$

$$k_{nf} = k_f\left(\frac{k_s + 2k_f - 2\phi(k_f - k_s)}{k_s + 2k_f + 2\phi(k_f - k_s)}\right). \tag{4e}$$

Here, ρ_f is density of the base fluid, ρ_s is density of the nanoparticles, k_f is thermal conductivity of the base fluid, k_s is thermal conductivity of the nanoparticles, γ_{nf} is the thermal expansion coefficient, γ_f is the thermal expansion coefficient of base fluid, ϕ is the nanoparticle volume fraction, and γ_s is the thermal expansion coefficient of the nanoparticles.

The following boundary conditions are to be employed:

$$u = u_w(r) = ar^n, \quad T = T_w, \quad at \;\; z = 0, \tag{5a}$$

$$u \to 0, T \to T_\infty, \quad as \;\; z \to \infty, \tag{5b}$$

in which u_w is the wall velocity, $a > 0$ is the stretching constant and $n > 0$ is the power-law index.

http://dx.doi.org/10.5772/intechopen.71224

Introducing the following similarity transformations:

$$\eta = \sqrt{\frac{a}{\nu_f}} r^{\frac{(n-1)}{2}} z,\ u = ar^n f'(\eta),\ \theta = \frac{T - T_\infty}{T_w - T_\infty},\ w = -ar^{\frac{(n-1)}{2}} \sqrt{\frac{\nu_f}{a}} \left(\frac{(n+3)}{2} f(\eta) + \frac{(n-1)}{2} n f'(\eta) \right). \quad (6)$$

Reynolds model of viscosity expression can be taken as:

$$\mu_f(\theta) = e^{-(\alpha\theta)} = 1 - (\alpha\theta) + O(\alpha^2), \quad (7)$$

where α is the viscosity parameter.

Using Eqs. (6) and (7) in Eqs. (1)–(5), the governing equations and boundary conditions are transformed as:

$$\frac{1 - (\alpha\theta)}{(1-\phi)^{2.5}} f''' + \frac{(-\alpha\theta')}{(1-\phi)^{2.5}} f''' + \left(1 - \phi + \phi \frac{\rho_S}{\rho_f} \right) \left\{ \frac{(n+3)}{2} f f'' - n(f')^2 \right\} \pm G_r \theta = 0, \quad (8)$$

$$\left(\frac{k_{nf}}{k_f} \right) \theta'' + \Pr \left(\frac{n+3}{2} \right) \left(1 - \phi + \phi \frac{(\rho c_p)_s}{(\rho c_p)_f} \right) [(f\theta')] = 0, \quad (9)$$

$$f(0) = 0, f'(0) = 1, f'(\infty) = 0, \theta(0) = 1, \theta(\infty) = 0, \quad (10)$$

where $\Pr = \frac{(\mu_0 c_p)_f}{k_f}$ is the Prandtl number.

The skin friction coefficients (C_{fx}) is defined as:

$$C_{fx} = \frac{\mu_{nf}(T)}{\rho_f {u_w}^2} \left(\frac{\partial u}{\partial z} \right)_{z=0}. \quad (11)$$

And the local Nusselt number (Nu_x) is defined as:

$$Nu_x = \frac{-x k_{nf}}{k_f (T_w - T_\infty)} \left(\frac{\partial T}{\partial z} \right)_{z=0}. \quad (12)$$

The dimensionless form of skin friction coefficients can be obtained as:

$$(\mathrm{Re}_x)^{1/2} C_{fx} = \frac{\mu_f(\theta(0)) f''(0)}{(1-\phi)^{2.5}}. \quad (13)$$

And the dimensionless form of skin friction coefficients can be obtained as:

$$(\mathrm{Re}_x)^{1/2} Nu_x = -\frac{k_{nf}}{k_f} \theta'(0). \quad (14)$$

3. Numerical scheme

Numerical solutions of ordinary differential Eqs. (8) and (9) subject to boundary conditions (10) are obtained using a shooting method. First we have converted the boundary value problem (BVP) into initial value problem (IVP) and assumed a suitable finite value for the far field boundary condition, i.e.$\eta \to \infty$, say η_∞. To solve the IVP, the values for $f''(0)$ and $\theta'(0)$ are needed but no such values are given prior to the computation. The initial guess values of $f''(0)$ and $\theta'(0)$ are chosen and fourth order Runge-Kutta method is applied to obtain a solution. We compared the calculated values of $f'(\eta)$ and $\theta(\eta)$ at the far field boundary condition η_∞(=20) with the given boundary conditions (10) and the values of $f''(0)$ and $\theta'(0)$, are adjusted using Secant method for better approximation. The step-size is taken as $\Delta\eta = 0.01$ and accuracy to the fifth decimal place as the criterion of convergence. It is important to note that the dual solutions are obtained by setting two different initial guesses for the values of $f''(0)$.

4. Numerical simulations and discussion

This section presents the numerical simulations for dimensionless velocity, temperature, skin friction, Nusselt numbers and streamlines under the influence of the flow parameters which are illustrated through the (**Figures 2–11**). **Table 1** is also given for thermophysical properties of base fluids and CNTs (MWCNT and SWCNT).

Figures 2 and **3** illustrate the velocity profiles for assisting and opposing flows where multi walled CNT is considered as nanoparticle and Kerosene is taken as base fluid. The Grashof number is fixed at 0.5. From all the figures, it is depicted that $f'(\eta)$ attains maximum values at $\eta = 0$ i.e. near the stretching sheet. It is clear from the transformation $\eta = \sqrt{\frac{a}{\nu_f}} r^{\frac{(n-1)}{2}} z$ that $\eta = 0$

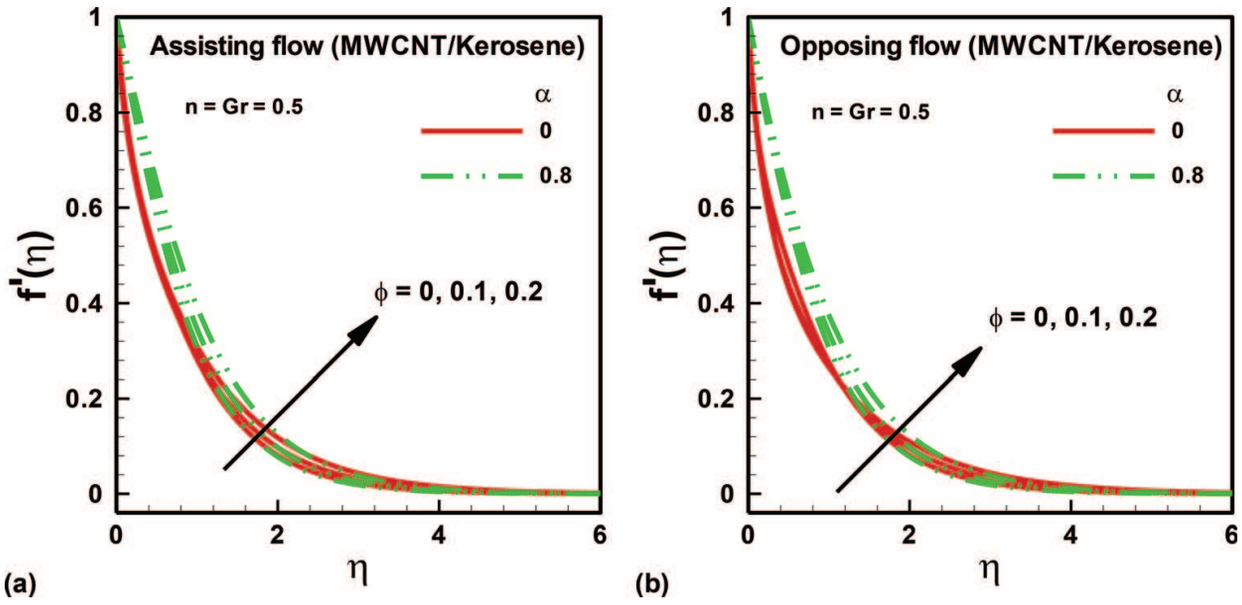

Figure 2. Velocity profile for different values of nanoparticle volume fraction and viscosity parameter: (a) assisting flow and (b) opposing flow.

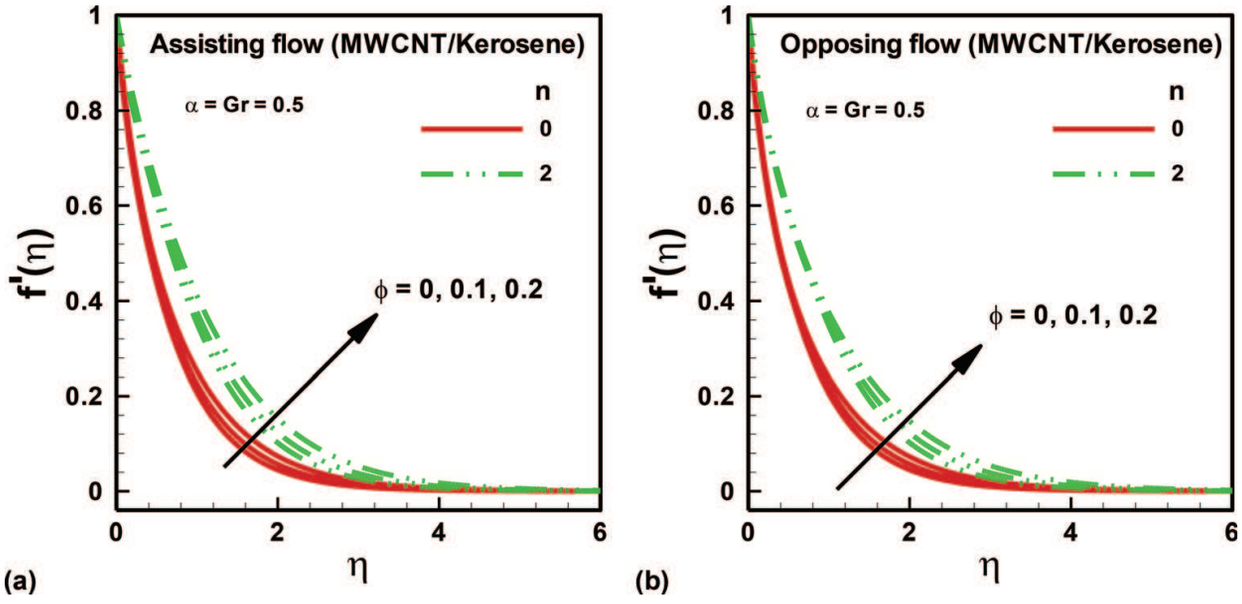

Figure 3. Velocity profile for different values of nanoparticle volume fraction and power law index: (a) assisting flow and (b) opposing flow.

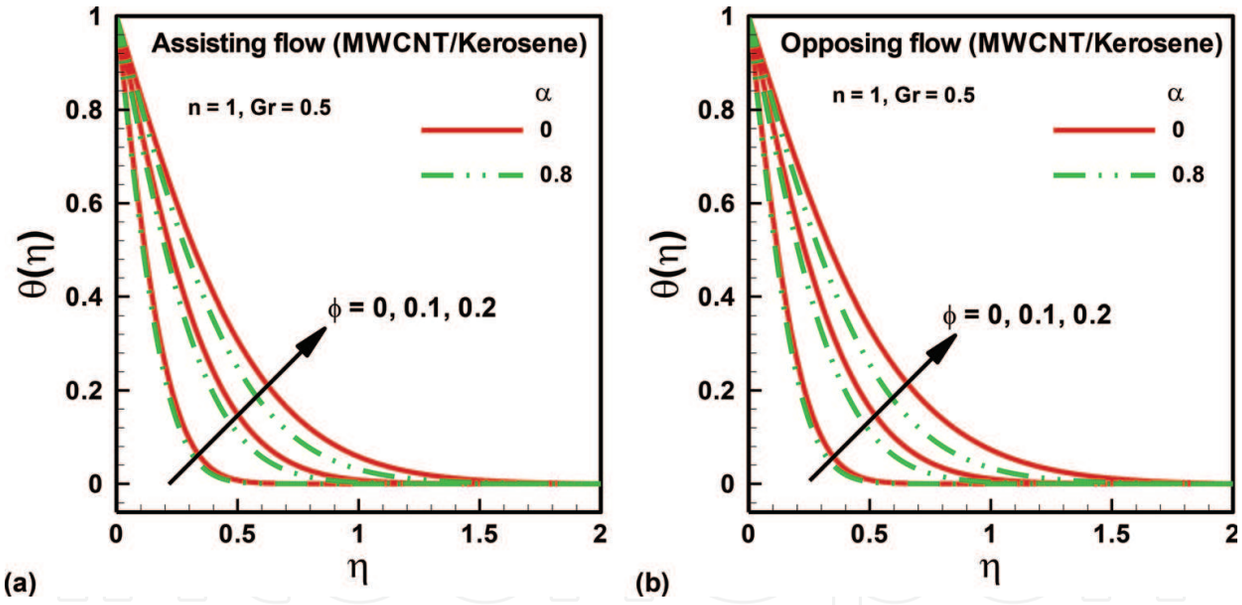

Figure 4. Temperature profile for different values of nanoparticle volume fraction and viscosity parameter: (a) assisting flow and (b) opposing flow.

at $z=0$. The curves show asymptotic nature long the η-axis. It is physically interpreted that the radial velocity diminishes when fluid is flowing away from the sheet. In **Figure 2** (**a** and **b**), the effects of nanoparticle volume fraction (ϕ) and viscosity parameter (α) on the velocity profiles for assisting flow and opposing flows are depicted and the value of power index is fixed at 0.5. It is inferred that with increasing the volume fraction parameter, the velocity slightly enhances for $\eta<4$ for both types of flows. It is also revealed that with increasing the magnitude of viscosity parameter, the radial velocity goes up $\eta<2$ for both types of flows. This is very clear from equation, $\mu_f(\theta)=e^{-(\alpha\theta)}=1-(\alpha\theta)+O(\alpha^2)$, that with increasing the magnitude of α, the

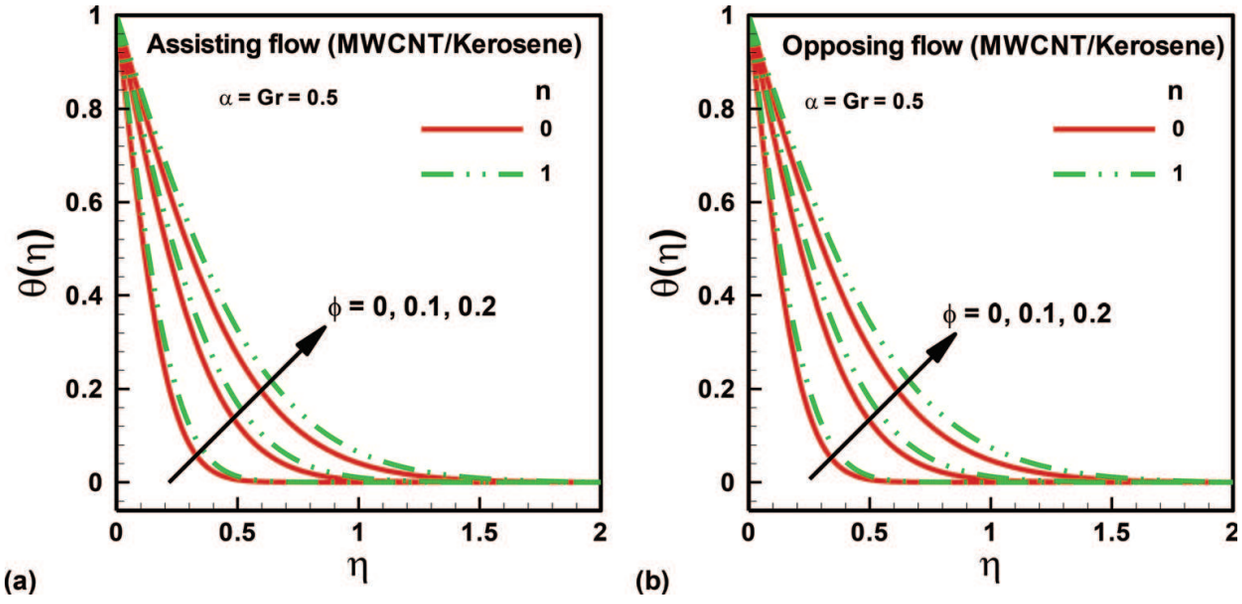

Figure 5. Temperature profile for different values of nanoparticle volume fraction and power law index: (a) assisting flow and (b) opposing flow.

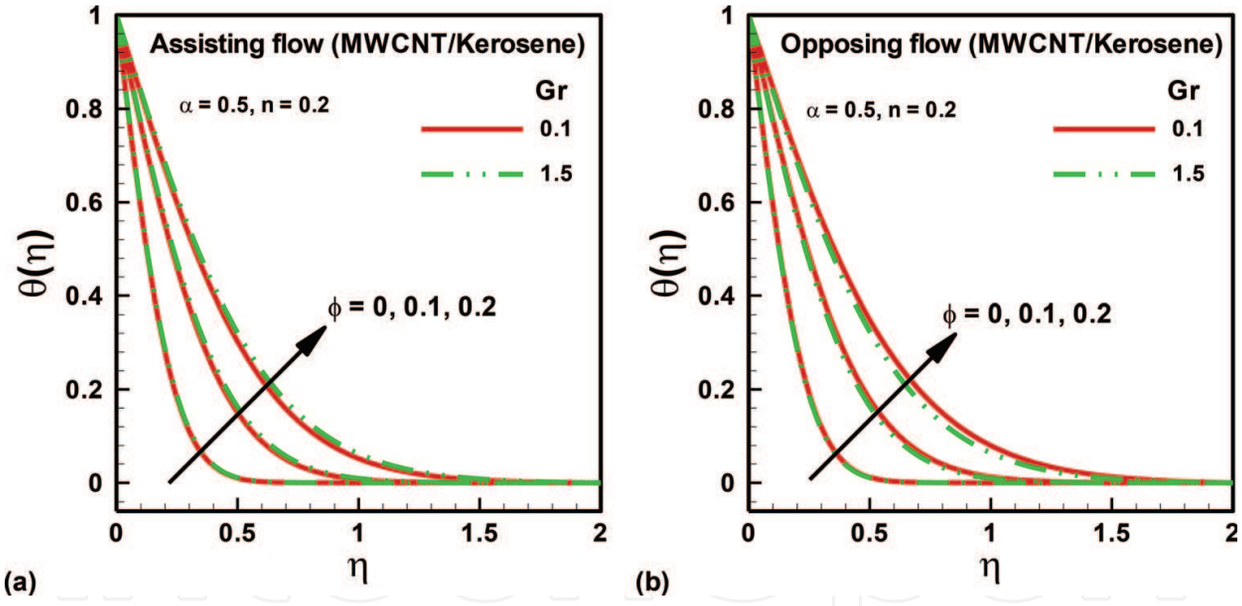

Figure 6. Temperature profile for different values of nanoparticle volume fraction and Grashof number: (a) assisting flow and (b) opposing flow.

viscosity will reduce. It is obvious that with increasing the viscosity of fluids, the shearing resistance will enhance and then velocity will go down. **Figure 3(a, b)** show that the effects of power law index (n) on velocity profile for both types of flows at fixed value of viscosity parameter 0.5. It is observed that the radial velocity rises with increasing the magnitude of power law index parameter. It is further noted that the velocity profile enlarges with increasing the nanoparticle volume fraction for all values of power law index and also viscosity parameter for both types of flows.

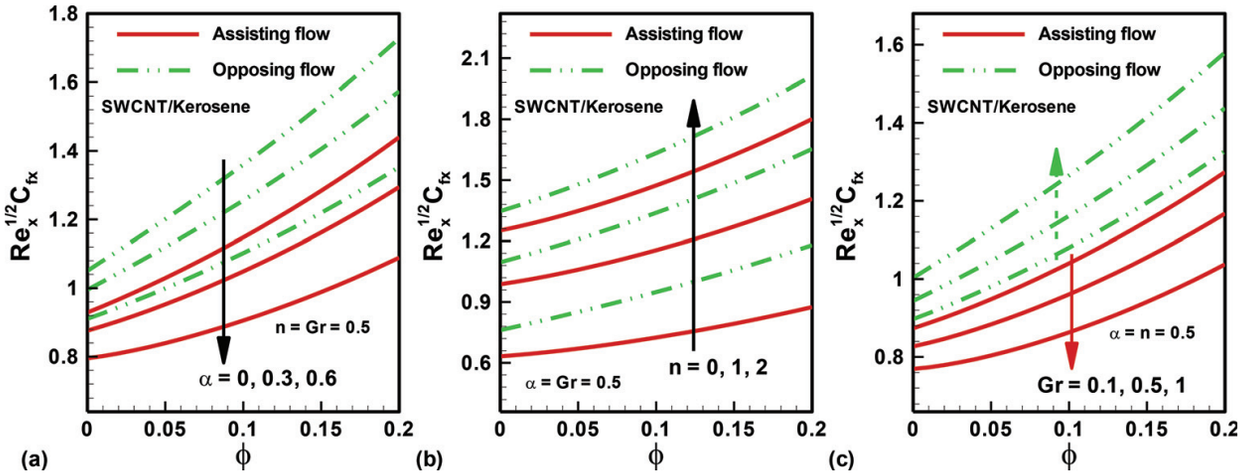

Figure 7. Variation of skin-friction coefficient against nanoparticle volume fraction for different values of (a) viscosity parameter, (b) power law index, and (c) Grashof number.

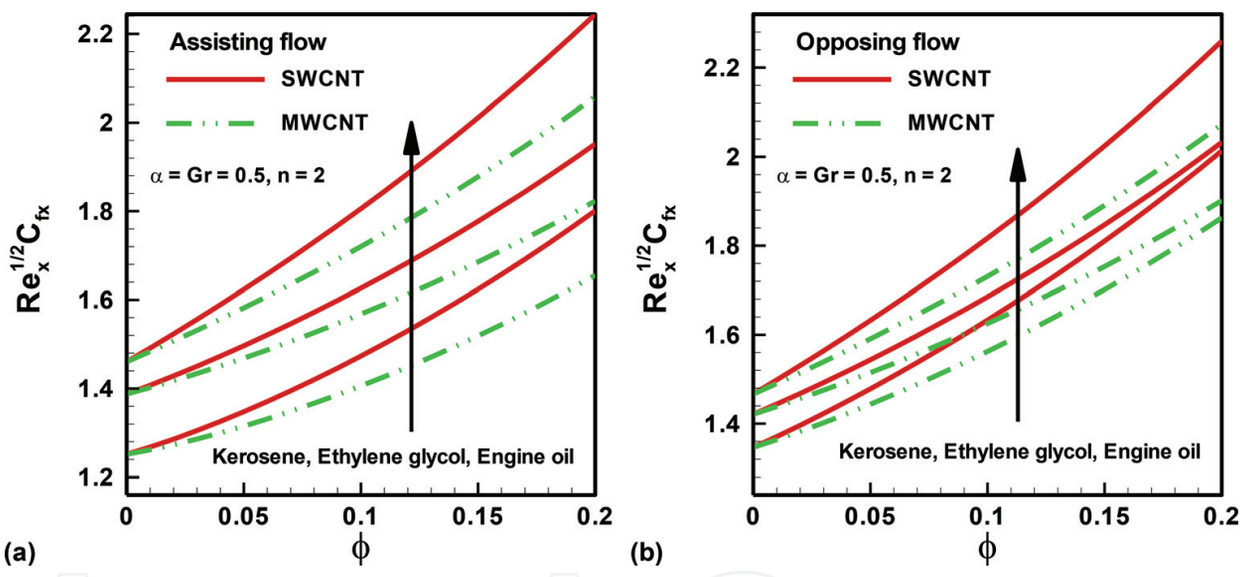

Figure 8. Variation of skin-friction coefficient against nanoparticle volume fraction for different base fluids and different CNTs: (a) assisting flow and (b) opposing flow.

The effects of viscosity parameter (α), power law index (n) and Grashof number (Gr) with various values of nanoparticle volume fraction (ϕ) on temperature profiles are depicted through **Figures 4–6**. For all computations, the nanoparticles and base fluid are considered as MWCNT and kerosene respectively. It is noticed that temperature is maximum at the wall of stretching sheet (i.e. $\eta = 0$ or $z = 0$). And when we see the temperature surrounding the sheet, it goes down significantly up to $\eta = 0.5$ and then after it is constant which is very close to zero. The patterns for temperature profile for assisting and opposing flows are similar. In **Figure 4**, the values of power index and Grashof number are considered as 1 and 0.5 respectively. **Figure 4** depicts that temperature falls with increasing the magnitude of viscosity parameter which is also very clear from the relation $\mu_f(\theta) = e^{-(\alpha\theta)} = 1 - (\alpha\theta) + O(\alpha^2)$ for both type flows (**Figure 4**(**a** and **b**)). The values of viscosity parameter and Grashof number are fixed as 0.5 in

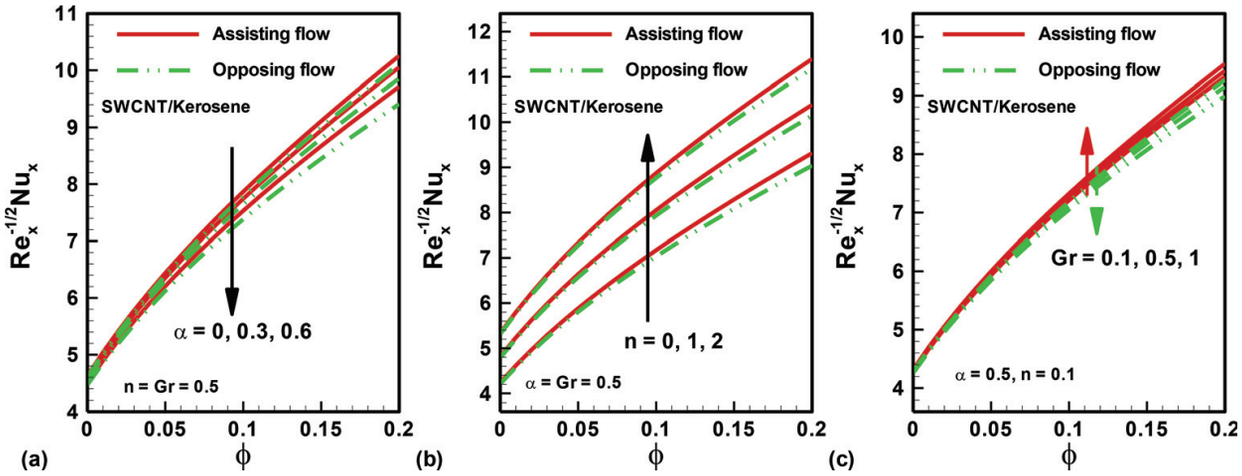

Figure 9. Variation of Nusselt number against nanoparticle volume fraction for (a) viscosity parameter, (b) power law index, and (c) Grashof number.

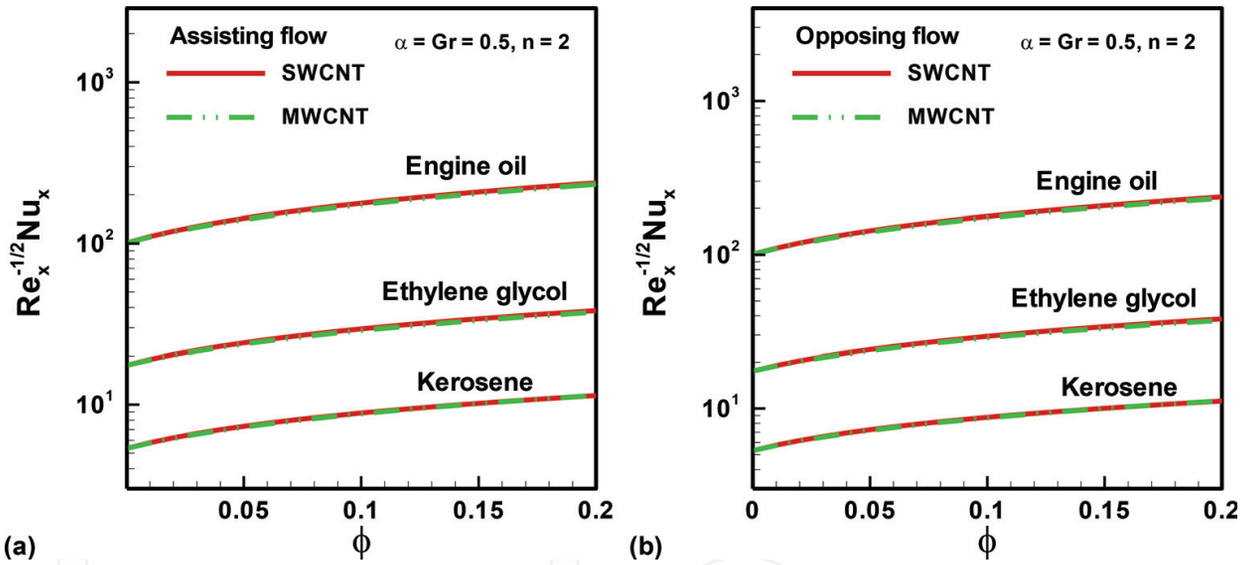

Figure 10. Variation of Nusselt number against nanoparticle volume fraction for different base fluids and also for different CNTs: (a) assisting flow and (b) opposing flow.

Figure 5. It is inferred that the temperature rises with increasing the power law index for different values of $\varphi = 0, 0.1, 0.2$ for both type flows (**Figure 5**(**a** and **b**)). The values of power law index and nanoparticle volume fraction are taken as 0.2 and 0.5 respectively in **Figure 6**. It is revealed that the temperature slightly increases with increasing the values of Grashof number for assisting flow, see **Figure 6a** however the temperature decreases with increasing the Grashof number for opposing flow, see **Figure 6b**. From **Figures 4–6**, it is also pointed out that the temperature goes up with increasing the nanoparticle volume fraction for all values of viscosity parameter, power law index and Grashof number, and also for both types of flows.

The variations in skin-friction coefficient against nanoparticle volume fraction are computed in **Figures 7** and **8** for assisting and opposing flows. It is found that the skin friction coefficient is

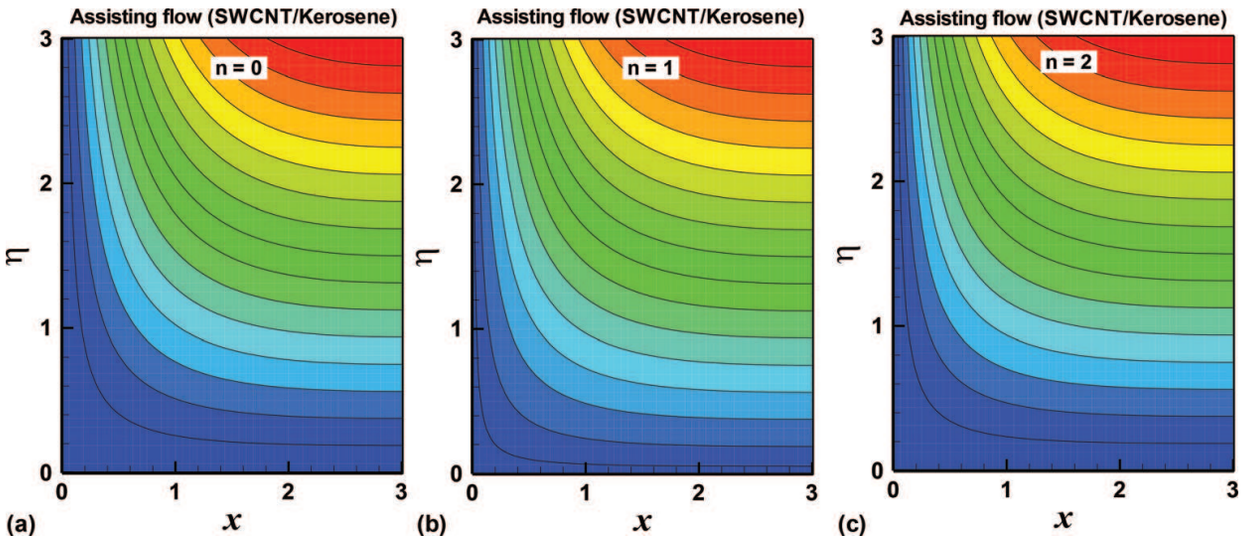

Figure 11. Stream lines for different values of power law index for $\alpha = 0.4$, $Gr = 3$, $\varphi = 0.3$.

Physical properties	Base fluid				Nanoparticles	
	Water	Kerosene	Engine oil	Ethylene glycol	MWCNT	SWCNT
ρ (kg/m^3)	997	783	884	1115	1600	2600
c_p (J/kg-K)	4179	2090	1910	2430	796	425
k (W/m-K)	0.613	0.15	0.144	0.253	3000	6600
Pr	6.2	21	6450	2.0363		

Table 1. Thermophysical properties of different base fluid and CNTs.

least at $\varphi = 0$ and it starts to enhance nonlinearly with increasing the values of nanoparticle volume fraction. In **Figure 7**, the nanoparticle and base fluids are considered as SWCNT and Kerosene respectively. The effect of viscosity parameter on skin-friction coefficient at fixed values $n = Gr = 0.5$ for both type of flows is presented in **Figure 7a**. It is observed that the magnitude of skin friction coefficient diminishes with increasing the viscosity parameter for both type of flows. The influence of power law index on skin friction coefficient is examined in **Figure 7b** at fixed values $\alpha = Gr = 0.5$ for both type of flows. It is depicted that skin friction coefficient extends for more values of power law index. **Figure 7c** is plotted for effects of Grashof number on skin friction coefficient at fixed values $\alpha = n = 0.5$ for both type of flows. It is revealed that magnitude of skin friction coefficient diminishes with increasing the magnitude of Grashof number for assisting flow and it increases with increasing the Grashof number for opposing flow.

Figure 8(**a** and **b**) are illustrated for the effects of different types of base fluids (kerosene, ethylene glycol and engine oil) and also effects of different CNTs on skin friction coefficient at fixed values $\alpha = Gr = 0.5$, $n = 2$ for assisting flow (**Figure 8a**) and opposing flow (**Figure 8b**). It is found that the magnitude of skin fraction is more for SWCNT in compare to MWCNT for all type of base fluids

and also for both type of flows. It is further depicted that skin friction is maximum for kerosene and minimum for engine oil for both types of CNTs and also for both types of flows.

Figures 9 and **10** are plotted to see the variations in Nusselt number against nanoparticle volume fraction both types of flows.

It is observed that the magnitude of Nusselt number is minimum at $\varphi = 0$. And it significantly increases with increasing the magnitude of nanoparticle volume fraction. The nanoparticle and base fluids are considered as SWCNT and kerosene respectively in **Figure 9**. **Figure 9a** illustrates that Nusselt number diminishes with increasing the magnitude of viscosity parameter for both type of flows at fixed values $n = Gr = 0.5$. **Figure 9b** shows that Nusselt number increases with increasing the power index both type of flows at fixed values $\alpha = Gr = 0.5$. **Figure 9c** reveals that Nusselt number increases with increasing the Grashof number for assisting flow however it reduces with increasing the Grashof number for opposing flow at fixed values $\alpha = n = 0.5$. **Figure 10**(**a** and **b**) are plotted to see the effects of Kerosene, Ethylene glycol and Engine oil and also effects of SWCNT and MWCNT on Nusselt number at fixed values $\alpha = Gr = 0.5, n = 2$ for both types of flows (**Figure 10a** and **b**). A very minor variation in Nusselt number for SWCNT and MWCNT nanoparticles is noted for assisting and opposing flows. A significant variation in Nusselt number for Kerosene, Ethylene glycol and Engine oil is pointed out where the Nusselt number is largest for Engine oil and smallest for Kerosene for both type of flows.

The stream lines are plotted through the **Figure 11**(**a**–**c**) to see the effects of power law index at fixed values $\alpha = 0.4, Gr = 3, \varphi = 0.3$ for assisting flow where SWCNT as nanoparticle and Kerosene as base fluid are considered. It is noted that stream lines go closer to each other with increasing the power law index.

5. Concluding remarks

A numerical investigation for boundary layer flow of CNTs nanofluids with temperature dependent viscosity over a circular stretching sheet is presented. Effects of Three types of base fluids, power law index, viscosity parameter, nanoparticle volume fraction and Grashof number on flow characteristics, and also skin friction coefficient and Nusselt number are discussed appropriately with numerical computations. The concluding remarks of present discussions are précised as:

- The nature of velocity and temperature profiles for assisting and opposing flows are similar for all values of pertinent parameters except Grashof number.
- The velocity boundary layer thickness elaborates with increasing the magnitude of nanoparticle volume fraction, viscosity parameter and power law index for both type of flows.
- The thermal boundary layer thickness expands with reducing the magnitude of viscosity parameter, power law index and nanoparticle volume fraction for both type of flows.
- The magnitude of skin friction coefficient enhances with increasing the nanoparticle volume fraction and power law index and it also enhances with decreasing the viscosity parameter for both type of flows.

- The sequence for skin friction coefficient of different nanoparticles is observed as: $\mathrm{Re}_x^{1/2} C_{fx}$ (SWCNT) > $\mathrm{Re}_x^{1/2} C_{fx}$ (MWCNT).
- The sequence for skin friction coefficient of different base fluids is also noted as: $\mathrm{Re}_x^{1/2} C_{fx}$ (kerosene) > $\mathrm{Re}_x^{1/2} C_{fx}$ (ethylene glycol)> $\mathrm{Re}_x^{1/2} C_{fx}$ (engine oil).
- The Nusselt number diminishes with increasing the viscosity parameter and it also diminishes with decreasing the power law index and nanoparticle volume fraction for both type of flows.
- The sequence for Nusselt number of kerosene, ethylene glycol and engine oil is noted as: $\mathrm{Re}_x^{1/2} Nu_x$ (kerosene) < $\mathrm{Re}_x^{1/2} Nu_x$ (ethylene glycol) < $\mathrm{Re}_x^{1/2} Nu_x$ (engine oil).

Author details

Noreen Sher Akbar[1]*, Dharmendra Tripathi[2] and Zafar Hayat Khan[3]

*Address all correspondence to: noreensher@yahoo.com

1 DBS&H CEME, National University of Sciences and Technology, Islamabad, Pakistan

2 Department of Mechanical Engineering, Manipal University Jaipur, Rajasthan, India

3 Department of Mathematics, University of Malakand, Dir (Lower), Khyber Pakhtunkhwa, Pakistan

References

[1] Choi, S. U. S. (1995). Enhancing thermal conductivity of fluids with nanoparticles. ASME, Publications-Fed, 231, 99-106

[2] Wang XQ, Mujumdar AS. Heat transfer characteristics of nanofluids: A review. International Journal of Thermal Sciences. 2007;**46**(1):1-19

[3] Das SK, Choi SU, Patel HE. Heat transfer in nanofluids—A review. Heat Transfer Engineering. 2006;**27**(10):3-19

[4] Mahian O, Kianifar A, Kalogirou SA, Pop I, Wongwises S. A review of the applications of nanofluids in solar energy. International Journal of Heat and Mass Transfer. 2013;**57**(2):582-594

[5] He Y, Jin Y, Chen H, Ding Y, Cang D, Lu H. Heat transfer and flow behaviour of aqueous suspensions of TiO_2 nanoparticles (nanofluids) flowing upward through a vertical pipe. International Journal of Heat and Mass Transfer. 2007;**50**(11):2272-2281

[6] Kim SJ, McKrell T, Buongiorno J, Hu LW. Experimental study of flow critical heat flux in alumina-water, zinc-oxide-water, and diamond-water nanofluids. Journal of Heat Transfer. 2009;**131**(4):043204

[7] Santra AK, Sen S, Chakraborty N. Study of heat transfer due to laminar flow of copper–water nanofluid through two isothermally heated parallel plates. International Journal of Thermal Sciences. 2009;**48**(2):391-400

[8] Ding Y, Alias H, Wen D, Williams RA. Heat transfer of aqueous suspensions of carbon nanotubes (CNT nanofluids). International Journal of Heat and Mass Transfer. 2006;**49**(1): 240-250

[9] Ko GH, Heo K, Lee K, Kim DS, Kim C, Sohn Y, Choi M. An experimental study on the pressure drop of nanofluids containing carbon nanotubes in a horizontal tube. International Journal of Heat and Mass Transfer. 2007;**50**(23):4749-4753

[10] Kumaresan V, Velraj R. Experimental investigation of the thermo-physical properties of water–ethylene glycol mixture based CNT nanofluids. Thermochimica Acta. 2012;**545**: 180-186

[11] Kumaresan V, Khader SMA, Karthikeyan S, Velraj R. Convective heat transfer characteristics of CNT nanofluids in a tubular heat exchanger of various lengths for energy efficient cooling/heating system. International Journal of Heat and Mass Transfer. 2013;**60**:413-421

[12] Walvekar R, Siddiqui MK, Ong S, Ismail AF. Application of CNT nanofluids in a turbulent flow heat exchanger. Journal of Experimental Nanoscience. 2016;**11**(1):1-17

[13] Akbar NS, Kazmi N, Tripathi D, Mir NA. Study of heat transfer on physiological driven movement with CNT nanofluids and variable viscosity. Computer Methods and Programs in Biomedicine. 2016;**136**:21-29

[14] Akbar NS, Abid SA, Tripathi D, Mir NA. Nanostructures study of CNT nanofluids transport with temperature-dependent variable viscosity in a muscular tube. The European Physical Journal Plus. 2017;**132**:1-10

[15] Crane LJ. Flow past a stretching plate. Zeitschrift für angewandte Mathematik und Physik (ZAMP). 1970;**21**(4):645-647

[16] Khan WA, Pop I. Boundary-layer flow of a nanofluid past a stretching sheet. International Journal of Heat and Mass Transfer. 2010;**53**(11):2477-2483

[17] Makinde OD, Aziz A. Boundary layer flow of a nanofluid past a stretching sheet with a convective boundary condition. International Journal of Thermal Sciences. 2011;**50**(7): 1326-1332

[18] Rana P, Bhargava R. Flow and heat transfer of a nanofluid over a nonlinearly stretching sheet: A numerical study. Communications in Nonlinear Science and Numerical Simulation. 2012;**17**(1):212-226

[19] Xu H, Pop I, You XC. Flow and heat transfer in a nano-liquid film over an unsteady stretching surface. International Journal of Heat and Mass Transfer. 2013;**60**:646-652

[20] Hussain ST, Nadeem S, Haq RU. Model-based analysis of micropolar nanofluid flow over a stretching surface. The European Physical Journal Plus. 2014;**129**(8):161

[21] Uddin MJ, Ferdows M, Bég OA. Group analysis and numerical computation of magneto-convective non-Newtonian nanofluid slip flow from a permeable stretching sheet. Applied Nanoscience. 2014;**4**(7):897-910

[22] Khan WA, Makinde OD, Khan ZH. Non-aligned MHD stagnation point flow of variable viscosity nanofluids past a stretching sheet with radiative heat. International Journal of Heat and Mass Transfer. 2016;**96**:525-534

[23] Hsiao KL. Stagnation electrical MHD nanofluid mixed convection with slip boundary on a stretching sheet. Applied Thermal Engineering. 2016;**98**:850-861

[24] Akbar NS, Tripathi D, Khan ZH, Bég OA. A numerical study of magnetohydrodynamic transport of nanofluids over a vertical stretching sheet with exponential temperature-dependent viscosity and buoyancy effects. Chemical Physics Letters. 2016;**661**:20-30

[25] Bhatti MM, Rashidi MM. Effects of thermo-diffusion and thermal radiation on Williamson nanofluid over a porous shrinking/stretching sheet. Journal of Molecular Liquids. 2016;**221**:567-573

[26] Zeeshan A, Majeed A, Ellahi R. Effect of magnetic dipole on viscous ferro-fluid past a stretching surface with thermal radiation. Journal of Molecular Liquids. 2016;**215**:549-554

[27] Majeed A, Zeeshan A, Ellahi R. Unsteady ferromagnetic liquid flow and heat transfer analysis over a stretching sheet with the effect of dipole and prescribed heat flux. Journal of Molecular Liquids. 2016;**223**:528-533

[28] Hayat T, Muhammad T, Shehzad SA, Alsaedi A. An analytical solution for magnetohydrodynamic Oldroyd-B nanofluid flow induced by a stretching sheet with heat generation/absorption. International Journal of Thermal Sciences. 2017;**111**:274-288

[29] Ellahi R, Hassan M, Zeeshan A. Shape effects of spherical and nonspherical nanoparticles in mixed convection flow over a vertical stretching permeable sheet. Mechanics of Advanced Materials and Structures. 2017;**24**(15):1-8

[30] Nayak MK, Akbar NS, Pandey VS, Khan ZH, Tripathi D. 3D free convective MHD flow of nanofluid over permeable linear stretching sheet with thermal radiation. Powder Technology. 2017;**315**:205-215

[31] Akbar NS, Khan ZH, Nadeem S. The combined effects of slip and convective boundary conditions on stagnation-point flow of CNT suspended nanofluid over a stretching sheet. Journal of Molecular Liquids. 2014;**196**:21-25

[32] Haq RU, Nadeem S, Khan ZH, Noor NFM. Convective heat transfer in MHD slip flow over a stretching surface in the presence of carbon nanotubes. Physica B: Condensed Matter. 2015;**457**:40-47

[33] Hayat T, Hussain Z, Alsaedi A, Asghar S. Carbon nanotubes effects in the stagnation point flow towards a nonlinear stretching sheet with variable thickness. Advanced Powder Technology. 2016;**27**(4):1677-1688

[34] Akbar NS, Khan ZH. Effect of variable thermal conductivity and thermal radiation with CNTS suspended nanofluid over a stretching sheet with convective slip boundary conditions: Numerical study. Journal of Molecular Liquids. 2016;**222**:279-286

IntechOpen